Exploration of Catalysis Activation Energy as a Function of Gold Nanoparticle Surface Morphology

By

Cristina F. Stefanescu

Submitted to the Department of Materials Science and Engineering in Partial Fulfillment of the Requirements for the Degree of

Bachelor of Science
at the
Massachusetts Institute of Technology

June 2008

Signature of Author:_____
Department of Materials Science and Engineering
May 16, 2008

Certified by:_____
Francesco Stellacci
Professor of Materials Science and Engineering
Thesis Supervisor

Accepted by:_____
Caroline A. Ross
Chair, Departmental Undergraduate Committee

This page was intentionally left blank.

Exploration of Catalysis Activation Energy as a Function of Gold Nanoparticle Surface Morphology

By

Cristina F. Stefanescu

Submitted to the Department of Materials Science and Engineering
on May 16th, 2008 in partial fulfillment of the
requirements for the Degree of Bachelor of Science in
Materials Science and Engineering

ABSTRACT:

The application of rippled gold nanoparticles with bi-ligand surface morphology as a catalyst was tested. The hydrolysis of 2,4-dinitrophenyl acetate (DNPA) served as the catalytic reaction being analyzed and the bi-ligand composition used was 16-mercapto-hexadecanoic acid to imidazole thiol (MHA to IT). The influence of temperature on catalytic reaction of DNPA with the MHA: IT system was tested for ligand rations of 2:1, 1:2, and 1:1 by monitoring the catalytic system on a UV-VIS spectrometer. Catalytic rate constants were obtained and found to increase with increased temperature. The measured catalytic rate constants were greatest overall for the 1:1 system, followed by the 1:2 system, and lastly the 2:1 system. The activation energy for each ligand-ratio system was measured and found to be 22.17 kJ/mol for the 2:1 system, 14.7 kJ/mol for the 1:2 system, and 26.52 for the 1:1 system. The 2:1 and 1:2 systems followed the trend of lower activation energy values for systems with faster rates; however the 1:1 system did not fit this trend as it resulted in the highest activation energy value as well as the fastest reaction rates.

This page was intentionally left blank.

Acknowledgements

This work was conducted in the Center for Materials Science and Engineering at the Massachusetts Institute of Technology in Professor Francesco Stellacci's lab group. I would like to thank Professor Stellacci for giving me the opportunity to work on this project and for his support throughout the year. I would also like to thank Benjamin Wunsch for his assistance with the acquisition and interpretation of results as well as his endless guidance in all aspects of the project. Erika Penzo also assisted with nanoparticle synthesis. In addition, I would like to thank the other members of the Stellacci group for their advice and assistance throughout the project, including the UROP students for some preliminary data collection.

TABLE OF CONTENTS

LIST OF FIGURES

LIST OF TABLES

1. Introduction

Over the last few years, nanomaterials have been gaining a large following because of their prospective applications from technology to catalysis. The growing interest in this field of research owes to the uniqueness and ease in customizability of their properties. Nanomaterials have not only proven to display improved material properties but have also demonstrated new ones as well. A promising new area of nanomaterial research is monolayer-protected metal nanoparticles (MPMN). Soluble in organic solvents due to the properties of the outer monolayer, these nanoparticles have potential for several interesting applications.

These metal nanoparticles are made up of a metallic core and a self-assembled monolayer referred to as the 'outer ligand shell'. It has been found that nanoparticles with a ligand shell of ordered phase-separated domains as small as 5Å can be synthesized and the ligand shells can be made of a composition of molecules. These nanoparticles with a mixed self-assembled monolayer (SAM) surface are fairly easy to synthesize and have been found to form phase-separated ordered domains in which each phase is a band or 'ripple'. More specifically, these synthesized nanoparticles display parallel domains that are ordered into ripples which band all the way around their metal core [1]. Successful results have been obtained of gold nanoparticles with mixed ligand-coating that spontaneously form these rippled domains on a subnanometer level. STM images have confirmed this rippled presentation that the domains formed in these mixed ligand shells. Figure 1a below provides a STM image of a synthesized gold nanoparticle coated with mixed ligands. This image demonstrates the rippled nature of the surface domains of these nanoparticles. Figure 1b provides a schematic drawing of a single rippled

nanoparticle which clearly denotes the rippled morphology of the nanoparticle ligand shell.

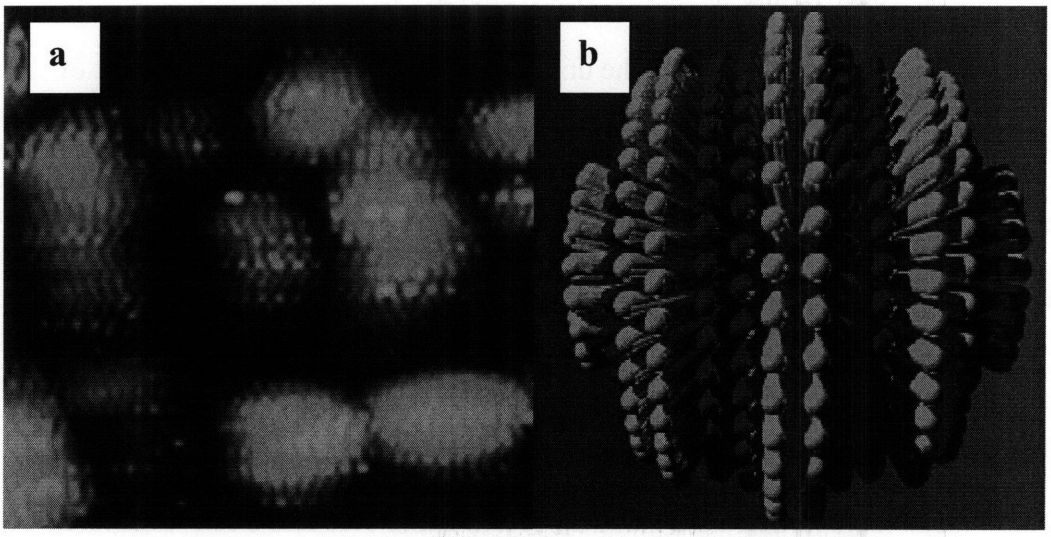

Figure 1: STM image and schematic drawing of phase ordered domains. a. STM image displaying the rippled phase-separated domains of gold nanoparticles synthesized with a 2:1 molar ratio of 1-octanethiol (OT) to mercaptopropionic acid (MHA). **b.** Schematic drawing of an MPMN with rippled phase-separated domains. The light bands represent the OT ligands and the dark bands represent the MHA ligands [1].

A useful characteristic of these nanoparticles is the ability to easily control the domain shape and dimensions of these rippled nanoparticles by adjusting the ligand composition or the particle core dimensions. More specifically, the height difference between ligands as well as the spacing between and shape of the domains can be controlled by altering the stoichiometry of the reagents used during the synthesis. Additionally, by adjusting the nanoparticle morphology, one is able to influence the solubility of the particle. The ability to somewhat nanostructure the surface of a nanoparticle allows one to have more control over the properties of those nanoparticles.

Upon examination of the behavior of these rippled nanoparticles, it was found that these nanoparticles possess an interesting surface energy profile. It is known that self-assembled monolayers (SAMs) are capable of providing specific surface energies to their surface layers [1]. Surface energy data for MHA: IT nanoparticles have recently been obtained and are summarized in Figure 2.

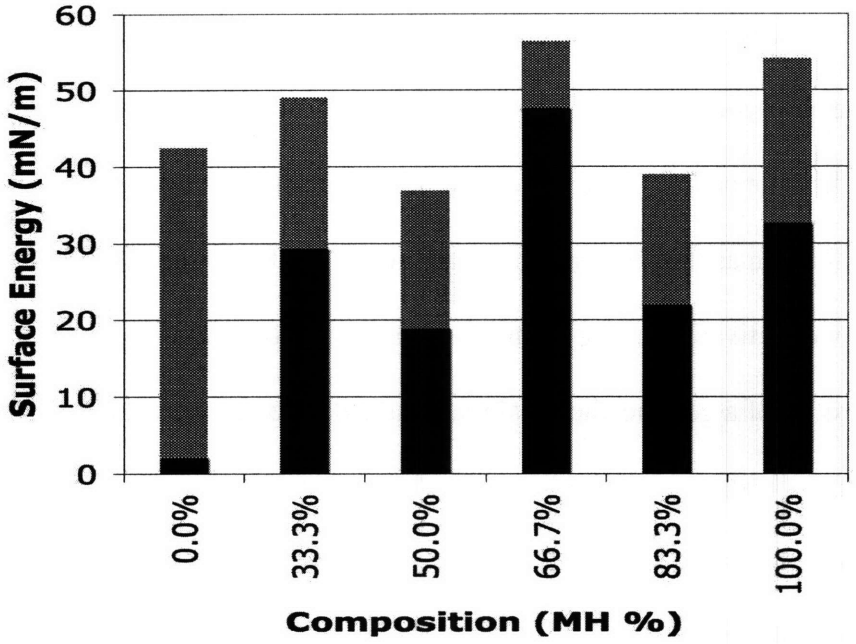

Figure 2: Surface energy values measured for nanoparticles of varying surface composition [6].

Although the reason behind this energy profile is not yet understood, the surface energy profile measured for these rippled nanoparticles appear to oscillate with surface composition. Considering that this shows the ability to vary the surface energy with surface morphology and also considering that surface energy is known to be a key factor

in catalysis reactions, an interesting idea can be raised about these nanoparticles and how they may be applied to enhance catalytic reactions.

2. Background

Catalysis is the increase in reactivity between two or more molecules by the presence of a third substance that remains unchanged by the reaction. The added substance, the catalyst, increases the reaction rate effectively by allowing a different reaction pathway to the end product. The route provided by the catalyst has a lower activation energy, E_a, than the pathway available without a catalyst. Because the activation energy, also known as the energy barrier, is directly related to the rate of a chemical reaction, a lower activation energy indicates a faster reaction rate [2].

The reaction profile of a generic chemical reaction is defined by an initial reaction state followed by a transition state that is higher in free energy and then terminated with the product state that returns to a lower free energy state. The activation energy of a chemical reaction is defined as the difference between this transition state and reaction state – it is the amount of energy required for the reactants to acquire in order for the chemical reaction to take place [2].

Catalysis is a very significant process to many areas of science, including the chemical industry as well as the fields of physics and environmental science. More importantly, catalysis is involved in most of the chemical reactions that occur in the human body as well as other living organisms. Without this process to assist many high-energy natural reactions, they would occur very slowly and, in some cases, not take place at all. Such biological catalysts occurring in nature are called enzymes.

Enzymes are macromolecules made of a polypeptide chain that serve as catalysts for biochemical reactions. They have a complex three-dimensional structure that is a result of spontaneous folding of its amino acid linear chains. An enzyme has very high specificity when catalyzing a reaction on a particular substrate [7]. Any enzyme contains an active site which constitutes the binding site of the enzyme and substrate. Recognition of the specific substrate and consequent binding and modification of the reaction mechanism at this active site takes place due to the particular shape and chemical properties of this site [7]. The basic structure of the active site is a pocket on the surface with a unique combination of residues that account for the high substrate specificity. These residues vary in terms of charge, hydrophobicity, and steric hindrance. A commonly acknowledged model used to describe the enzyme-substrate interaction is the induced fit model which describes the substrate binding to the rigid active site while also interacting fluidly with the amino acid side chain residues on the walls of the active site.

Rippled nanoparticles in organic catalysis serve as an interesting comparison to enzymes in enzymatic catalysis since the nanoparticles and enzymes both share the same structural and chemical properties. They both are hard objects with unique surface properties. The appearance of the ordered domains of rippled nanoparticles roughly resembles the active sites of enzymes. Considering this point as well as the earlier point noted about surface energy properties, an interesting possibility is raised to investigate the development of nanoparticles as catalytic platforms, similar to that of enzymes. (Rippled nanoparticles in catalysis could perhaps even lead to a greater understanding of the basic principles of enzyme chemistry and enzymatic catalysis.)

Because the bi-ligand surface morphology is the unique aspect of these new rippled nanoparticles, a more specific area to focus on is not simply the investigation of rippled nanoparticles as catalysts, but more specifically how their domain morphology affects the catalysis. By comparing the activation energy for catalytic systems of rippled nanoparticles with varying surface morphology, it is possible to explore the effect that a different surface composition has on the catalytic ability of these novel nanoparticles.

In order to investigate the idea of rippled nanoparticles in a catalytic system, it was necessary to first find a catalytic system that could be used as a model. The work achieved by Scrimin, *et al.* with functionalized gold nanoparticles as catalysts was found to provide a successful catalytic mechanism with gold nanoparticles [4]. The specific reaction that Scrimin, *et al.* consider is the hydrolysis of 2,4-dinitrophenyl acetate (DNPA). A base and water are necessary for this chemical reaction. Gold nanoparticles functionalized with a monolayer of 1:1 dodecane to N-methylimidazole (imidazole) were synthesized with carboxylate groups being presented on their outer surface. They served as a catalyst in the hydrolysis of DNPA in a 6:4 methanol to water solution, in which the nanoparticles were completely soluble. Imidazole was chosen as a suitable surface ligand because of its previously proven success as a catalyst in a hydrolytic system [4]. This reaction was performed over various pH's, ranging from 4.5-7.2. Each trial was monitored by a UV-VIS spectrometer and the rate constant was obtained. As a control case, the reaction was also run and monitored at various pH's with acetyl-N-methylhistamine, a monomeric catalyst [4]. Figure 3 displays the two resulting fitted curves of the second order rate constant versus pH obtained by Scrimin, *et al.* for their nanoparticle as well as monomeric catalyst systems.

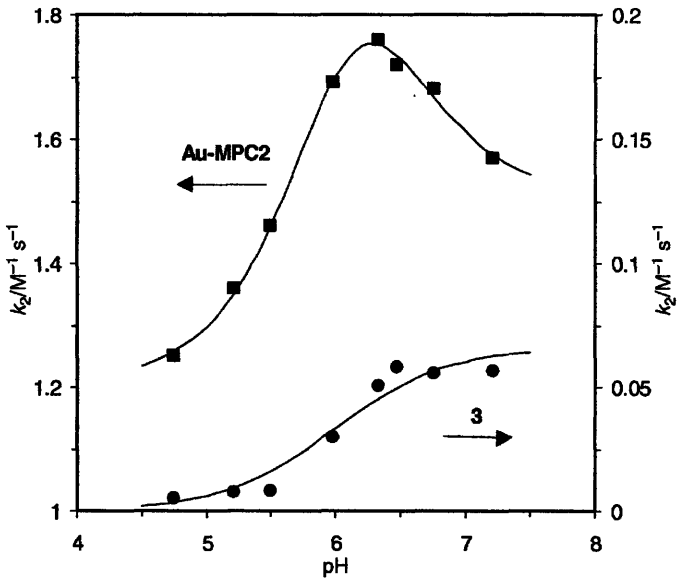

Figure 3: Rate constant versus pH for catalytic trials by Scrimin, *et al.* The top curve is the second order rate constant dependence on pH for the hydrolysis of DNPA with gold nanoparticles. The bottom curve is the second order rate constant dependence on pH for the hydrolysis of DNPA with the control catalyst [4].

This plot clearly shows the increase in reaction rate for DNPA hydrolysis in the presence of the functionalized Au-nanoparticles as compared to the monomeric control case. An interesting dependence of the rate constant on pH is also displayed.

The catalytic system proposed and tested by Scrimin, *et al.* serves as a successful example and suitable system to apply the idea of the application of rippled nanoparticles to a catalytic system. By replacing Scrimin, *et al.*'s functionalized gold nanoparticles from the system with the rippled gold nanoparticles discussed earlier, it is possible to explore the possibility of these novel rippled nanoparticles in a catalytic system.

3. Project Outline

For this project, the focus is on nanoparticle syntheses with a bi-ligand surface layer of 16-mercapto-hexadecanoic acid (MHA) and 10-mercapto-undeca-1N-imidazole (imidazole thiol IT). The MHA has a terminal carboxylic group and the IT acts as an organic catalyst. MHA is a useful organic compound to work with because it is helpful for making things soluble in water since it is fully charged and water soluble; this is an important characteristic since we need something to assist the catalyst with the hydrolysis reaction of DNPA. MHA is also a good compound on which to focus since the reaction rate for a hexadecanoic acid and IT ligand composition has been found to have a higher reaction rate over other tested compositions, such as 1-octanethiol (OT) and IT. The MHA: IT composition has the MHA longer ligands positioned with the shorter IT ligands on the surface of the nanoparticle. (This is in contrast with the OT: IT system where the catalyst extends further out rather than being stuck on the nanoparticle surface.) The synthesis with a 1:1 ligand ratio is the one that is the most rippled. While not as truly rippled as the 1:1, the 1:2 and 2:1 ligand ratios are also considered rippled for this project. It has been found that the MHA: IT system for the three afore mentioned ligand ratios display different catalytic rate constants at 25 C. These data are provided in Figure 4.

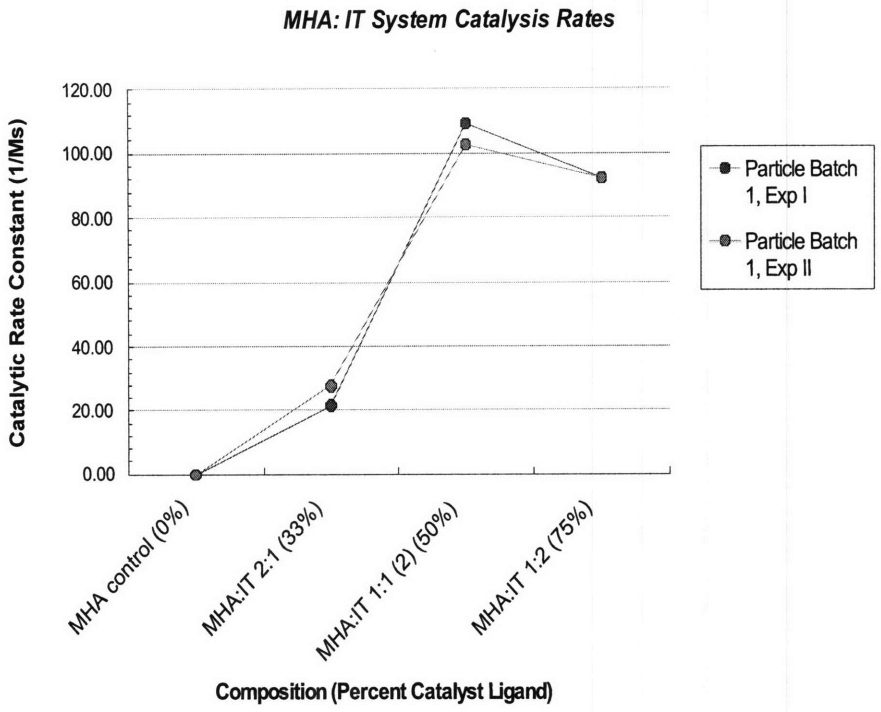

Figure 4: Catalytic Rate Constants, k_{cat}, obtained for MHA: IT nanoparticle systems with varying percentage of catalyst ligand, IT [5].

From Figure 4, it is evident that MHA: IT of 1:1 has the fastest k_{cat} value whereas that for 1:2 is a little slower and 2:1 is the slowest. This trend proves an interesting point about this rippled nanoparticle system because it demonstrates that these higher reaction rate constants are due to the presence of both ligands, not simply the catalyst – if the catalyst were the only important factor causing the interesting kinetic results, then it would make sense for the nanoparticles with higher concentration of catalyst (the 1:2 system) to have the fastest catalytic reaction rate.

By exploring the influence of temperature on the catalytic reaction of DNPA with the MHA: IT rippled nanoparticles of various ligand ratios, the kinetic parameters can be obtained by monitoring the reaction on a UV-VIS spectrometer and the activation

energies can be calculated and compared between MHA: IT nanoparticles of different ligand ratios, and therefore, different surface morphologies.

For analysis of the kinetic runs and extraction of the kinetic parameters, some basic kinetics must be understood. The first order rate constant, k, for a given reaction can be determined from the Arrhenius equation:

$$k = A\, e^{(-Ea/RT)} \qquad (1)$$

where A is a proportionality constant, also known as the jump factor, which accounts for several factors including the orientation of and number of collisions between reacting particles. Ea is the activation energy, R is the ideal gas constant, and T is the temperature. This equation demonstrates the relationship between activation energy and reaction rate. It is clear that the rate of reaction will increase exponentially as the activation energy is reduced [2].

While the Arrhenius equation describes the dependence of the rate constant on the activation energy value, it also gives the dependence of the rate constant on temperature. Generally, the use of a catalyst leads to an increase in the reaction rate with an increase in the temperature [2]. When studying the effect of temperature on a chemical reaction rate, an Arrhenius plot is often used. This plot is achieved by graphing the natural log of the rate k versus 1 over the temperature (1/T) [3]. For this plot, the Arrhenius equation can be represented in the form:

$$\ln(k) = \ln(A) - \frac{E_a}{R}\left(\frac{1}{T}\right) \qquad (2)$$

If the reaction is a single-rate thermodynamic process, the Arrhenius plot will result in a straight line. From this plot, one can extract the activation energy value as well as the

proportionality constant A since the slope is equivalent to $-E_a/R$ and the y-intercept is equal to ln(A) [3].

4. Description of work and experimental procedures

This project consisted of three main components: learning and executing gold nanoparticle synthesis, reproducing data depicted in Figure 3 by Scrimin, *et al.*, and performing catalysis trials at different temperatures to analyze the resulting kinetic parameters and calculate the activation energy. A table of chemicals used as well as their manufacturers is included in the appendix.

4.1 Nanoparticle synthesis

For the synthesis of gold nanoparticles with various surface ligand with surface layer of IT and a second ligand, the following set method was applied. A 250 or 500 mL round bottom (RB) flask with a stir bar was set up in a large glass bath container. The bath was packed with ice and filled ¾ high with water. The flask set up was placed on a stir plate. Considering a 0.18 mmol total of ligand required for the synthesis, the total amount was split and determined according to our desired bi-ligand composition. (For example, for a 1:1 synthesis, 0.9 mmol of each ligand would be used.) Along with measuring out the appropriate ligand amounts, 70.9 mg of Gold(III)hydrogentetrachloride (HAuCl4) and 75.66 mg Sodium borohydride (NaNH4) were weighed out and placed in individual 20 mg vials. For the IT ligand, it was taken from a stock solution of 50 mL IT in 1mL 100% ethanol. The correct amount of IT stock solution to use in order to gain the desired molar amount was determined by considering the molecular weight of IT (254.44

g/mol). 100 mL of pure ethanol was measured into a beaker. A small amount of this ethanol was poured into the vial of gold salt until about half way to make sure all particles were dissolved. This gold-ethanol solution was then added to the large flask. The vial was rinsed several times with the remaining ethanol from the beaker and sequentially added to the flask. (This was to ensure the addition of all gold salt pellets to the flask's contents.) The same ethanol washing procedure was used to add the two thiol ligands to the flask. Any remaining ethanol from the original 100mL was added to the flask and the flask was then left to stir for at least ten minutes. Another 100 mL of pure ethanol was measured into a beaker and set up on a mixer with a stir bar. The NaBH4 was dissolved into the pure ethanol.

A 60 mL syringe without the plunger and with a needle was set up above the large flask and 1-2 mL of the NaBH4 solution was added to the syringe. Once this solution completely dropped down into the flask, additional small amounts of the NaBH4 solution were added to the syringe two more times. After this, the remaining NaBH4 solution was added to the flask. The flask solution should then appear a dark brown from a previous golden color. After the solution completely dripped down into the flask (after about 1-2 hours), the flask was capped and placed in the freezer to precipitate. Nanoparticle precipitation usually takes a few days to a week.

Upon precipitation, the nanoparticle solution was purified and filtered by the following process. A rotavap machine was used to evaporate off most of the 50 ml solution down to about 5-6 ml. The concentrated nanoparticle solution was transferred into several Eppendorf tubes, each with 500ul of the nanoparticle solution. 1000ul of toluene was added to each tube. The Eppendorf tubes were then set in the centrifuge for

ten minutes at 5 kRPM. Then, after removing all supernatant, the tubes were filled to the top with toluene, sonicated to mix all contents, and underwent centrifugation again. This process of centrifuging and cleaning was repeated at least 5 times. After removing the last round of toluene from the microcaps, 500ul of ethanol was added to each one. All tubes were sonicated to disperse contents and then 1000ul of Millipore water (miH20) was added to each tube. These tubes were then sonicated and run through the centrifuge. This water washing process was repeated a second time. The water was then removed and the centrifugate from each tube was dispersed with an overall total of 3 ml ethanol. This stock nanoparticle solution was left to stir for at least 24 hours in order to ensure good dispersion.

4.2 Preparation and running of catalysis reaction

Using the prepared synthesized nanoparticles, a catalytic reaction was set up with the following set procedure. Two identical buffer solutions were made by creating a mixture of 1 M HEPES buffer stock and 0.5 M MES buffer stock totaling to 30mM and adding it to 3 ml water. Depending on the desired pH, the ratio of HEPES to MES was adjusted accordingly. Table 1 below provides the exact portions of each buffer added together to acquire the buffer solution of a particular pH.

HEPES (uL)		MES (uL)	~pH (paper)	~pH (meter)
H100	90	0	7	7.1
H95M5	86	9	~6.75	
H90M10	81	18	6.5	6.8
H80M20	72	36	5.75	6.4
H70M30	63	54	5.5	6.0
H60M40	54	72	5.25	5.9
H50M50	45	90	4.75	5.6
H40M60	36	108	4.5	5.4
H30M70	27	136	4.25	5.0
H20M80	18	154	4.1	4.9
H10M90	9	162	~ 4	4.5
M100	0	180	4	3.7

Table 1: Amounts of HEPES and MES buffer used for solutions of different pH

The catalyst solution was prepared by adding 50 ul of synthesized nanoparticle stock to one of the buffer solutions. (The other buffer solution is used later for blanking.) It is noted that the mixing order is important – it is necessary to mix the water and buffer together first before adding the nanoparticles, because otherwise the particles seem to irreversibly aggregate and become undissolvable. This catalyst solution is then added to micro-centrifuge tubes and run through the centrifuge for ten minutes at 5 kRPM. Then, after removing the supernatant from the tubes, the solution was placed into a vile ready for a catalysis trial.

Having prepared all of the solutions necessary for running the catalysis trial, the UV-VIS spectrometer was set up. A Starna Cell Quartz cuvette was cleaned with Aqua Regina and rinsed with acetone and ethanol. After leaving the UV-VIS light bulbs on to warm up for at least half an hour, the buffer solution for blanking was then added to the

cuvette and set in the machine. The spectrometer was set to trace 400, 360, and 253 nm wavelengths and the run time and sampling cycle time were also specified. A blank reading was taken of the buffer solution which was then removed from the cuvette. The catalyst solution was then poured into the cuvette and the trial was then set to start running. After ten minutes, 42.6 ul of the DNPA stock solution (2 mg DNPA in 5 ml acetonitrile) were added to and stirred in the cuvette and the spectrometer was left to monitor the ensuing catalytic reaction. In order to check that 100% product formation was reached at the end of each run, 100 ul of KOH solution (1 mmol/mL of KOH in milipore-water) was added to the cuvette at the end of the run and a sample spectrum was taken. This particular amount of KOH is used since it has been found to completely quench the DNPA concentration that was used.

4.3 Catalytic trials performed

Using the two main procedures described above, several catalytic trials were set up and performed. The first catalytic runs set up were as follows. In order to verify the catalytic reaction reported in the bottom curve of Figure 3 of Scrimin, *et al.*'s plot, several catalysis trials were set up with 1-butylimidazole serving as the catalysis in water. In order to set up these runs with the control instead of the nanoparticle catalyst solution, a few adjustments were made from the procedure of setting up and running a catalytic trial in section 4.2. The procedure was the same as described in section 4.2 except for a few aspects: the catalyst solution was prepared by adding 12.3 ul 1-butylimidazole to 1 ml acetonitrile, and the 42.6 ul DNPA were added to the prepared buffer solution. Upon starting the catalysis run on the UV-VIS spectrometer, 10 ul of the catalyst solution were

then added to the cuvette. The run time was set to 12 hours and the cycle time to 60 seconds. Several 1-butylimidazole catalysis trials were performed, each one at a different pH and therefore using a different buffer solution. The buffer solutions used ranged from about a pH of 4 to a pH of 7.

Catalysis runs at various pHs were also performed with a OT:IT 1:2 synthesized nanoparticle catalyst solution. These trials were run in order to see if the results gained with the rippled nanoparticles were comparable to those gained by Scrimin, *et al.* in Figure 3's top curve with non-rippled nanoparticles. The run time was set to 3600 seconds and the cycle time to 60 seconds.

The next set of catalysis trials was run at a set pH but at various temperatures for a few types of MHA: IT nanoparticle syntheses. Prior to starting the trial, the temperature was set to the desired degree. Using the catalysis run method in section 4.2, we set up each trial by making a buffer solution of 100% HEPES corresponding to a pH of about 7. (All runs were run at a pH of ~7 for two reasons: we wanted to work in a pH that was not too basic (where the rate is too slow) but that was also still within the basic range since it is necessary for both the hydrolysis reaction and produces good acid-base catalysis reactions. The run time was set to 7200 seconds and the cycle time to 20 seconds. The blank was taken at the same temperature on which the trial was being run; however, the sample taken when quenching with KOH at the end of each run was taken at 25C, room temperature. One set of trials performed over a range of temperatures (roughly from 8C to 75C) were run with MHA: IT 1:2 nanoparticles. Another set of trials was also run with MHA: IT 1:1 nanoparticles.

4.4 Calculations

In order to obtain the activation energy corresponding to the different nanoparticle syntheses, several calculations must be made. The obtained kinetic curves were fitted using the advanced fitting tool in OriginPro 7.0(2). An exponential fit was chosen that follows the following equation:

$$y = A + B(1-\exp(-t/t_{ob})) \qquad (3)$$

where A and B are scaling coefficients, t is the time, and t_{ob} is the observed time constant. When fitting, it was important to obtain a minimum R^2 value of 0.99. The fitting yields the corresponding time constant for that curve. A second order equation was used since it gave a better fit – therefore, two time constant values were given for each fitted curve. The observed rate constant, k_{ob}, was given by calculating $1/t_{ob}$. Since the goal is to observe the relationship of temperature to the catalytic rate constant, k_{cat}, it was necessary to convert the k_{ob} values to their corresponding k_{cat} values.

k_{ob} and k_{cat}, in units of 1/second, can be related by the following expression:

$$k_{cat} \sim k_{ob} / M_{cat} \qquad (4)$$

where M_{cat} is in mol/L and refers to the nanoparticle concentration. The correct full expression is actually $k_{cat} = (k_{ob} - k_{nocat})/ M_{cat}$, where k_{nocat} refers to the rate constant without the catalyst. However, because it is known empirically that k_{nocat} is over an order of magnitude smaller than k_{ob}, the expression in equation (4) is used. In order to determine the nanoparticle concentration, and thus the catalyst concentration, the initial plasmon height of each trial was used. This plasmon value was found to be the difference between the maximum absorbance at around 520-560nm and at 850nm. (The value at

850nm wavelength is considered to be the actual zero of the spectrum.) By dividing this plasmon absorbance value by an extinction coefficient representing the imaginary part of the dielectric constant, the resulting value is the concentration of nanoparticles in mol/L. The extinction coefficient is a factor specific to a particular nanoparticle synthesis type that takes into account the particle size and distribution, and it is given by the equation below:

$$\ln(\varepsilon) = \ln(D)k + a \qquad (5)$$

where ε is the extinction coefficient, D is the mean diameter of the particles in nm, k equals 3.3211, and a equals 10.80505.

By using this calculated nanoparticle concentration value, it was possible to use equation (4) and gain the k_{cat} value. An Arrhenius plot was created from the k_{cat} values and their corresponding run temperatures. By making this plot, a linear trend line was employed and the slope was determined and gave the activation energy value. The jump factor was also determined from the y-intercept value.

5. Results

The control curve obtained with 1-butylimidazole as a catalyst is provided in Figure 5 below. While this trial did not display the same peak structure at the pKa value, it did successfully reproduce the Scrimin, *et al.* results from Figure 3 in the sense that it reproduced the superiority of the nanoparticles used over the molecular ligand in the reaction. (Although it is not yet understood why the pKa peak structure was not reproduced, it is suspected to be related to the difference in the catalyst molecule being used.) The curve in Figure 5 also confirmed the catalytic reaction of hydrolysis of DNPA with an imidazole.

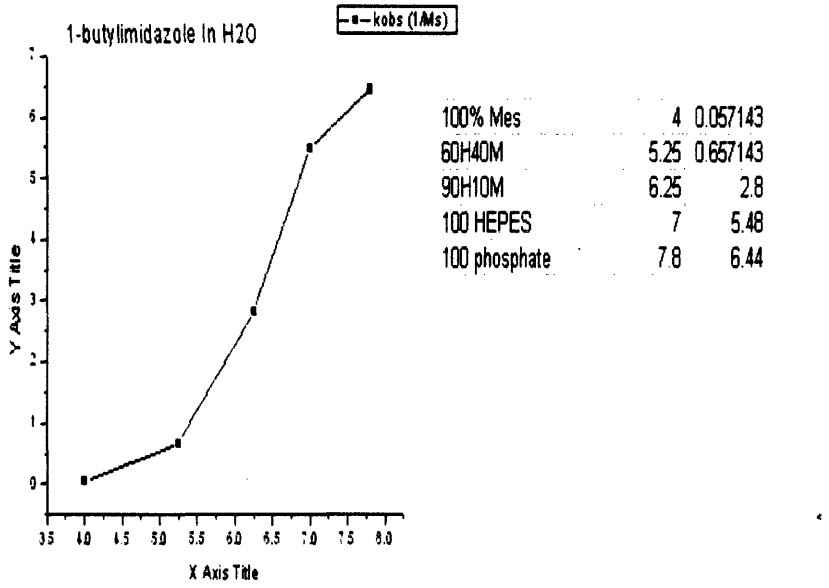

Figure 5: Control run of 1-butylimidazole in H_2O

The set of catalysis runs with OT : IT 1:2 nanoparticles at various pHs are presented in a rate constant vs. pH plot in Figure 6. This plot also includes curves obtained for OT: IT systems of other ligand-ratios previously tested in the Stellacci Lab. The plot in Figure 6 does not show a similar curve with a peak in the middle like that obtained in Figure 3.

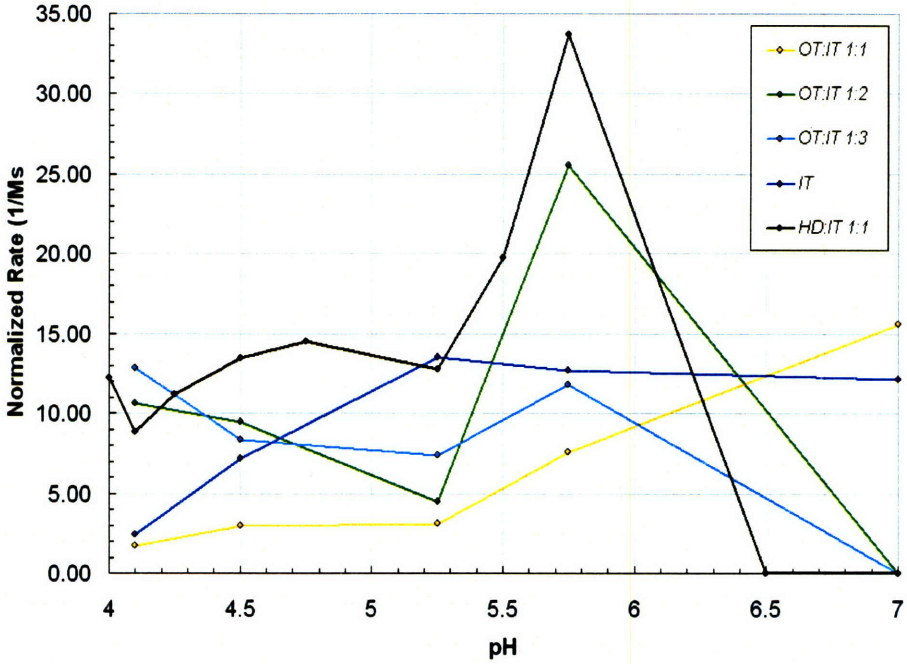

Figure 6. Experimental rate k versus pH for various nanoparticle systems [5].

The set of catalysis trials done at varying temperatures were plotted on one graph of the percent product vs. time and are presented in Figure 7. A plot is presented for the trials with MHA: IT 1:2 as well as 2:1 and 1:1. It is important to note that the plots in Figure 7 were normalized by using the spectrum obtained from each run after quenching the DNPA with KOH.

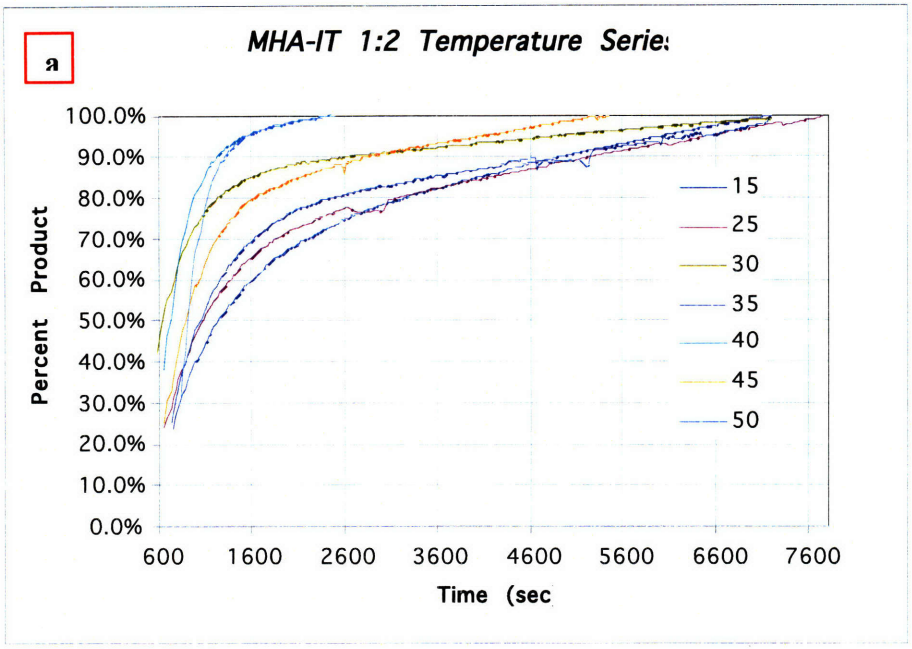
a
MHA-IT 1:2 Temperature Serie
100.0%
90.0%
80.0%
70.0%
60.0%
50.0%
40.0%
30.0%
20.0%
10.0%
0.0%
Percent Product
600
1600
2600
3600
4600
5600
6600
7600
Time (sec
15
25
30
35
40
45
50

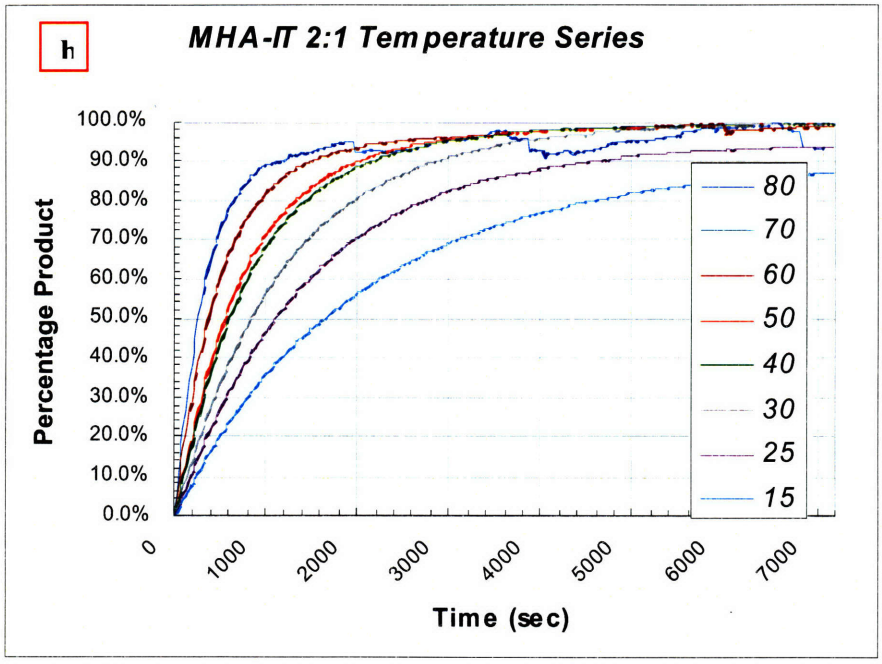
h
MHA-IT 2:1 Temperature Series
100.0%
90.0%
80.0%
70.0%
60.0%
50.0%
40.0%
30.0%
20.0%
10.0%
0.0%
Percentage Product
0
1000
2000
3000
4000
5000
6000
7000
Time (sec)
80
70
60
50
40
30
25
15

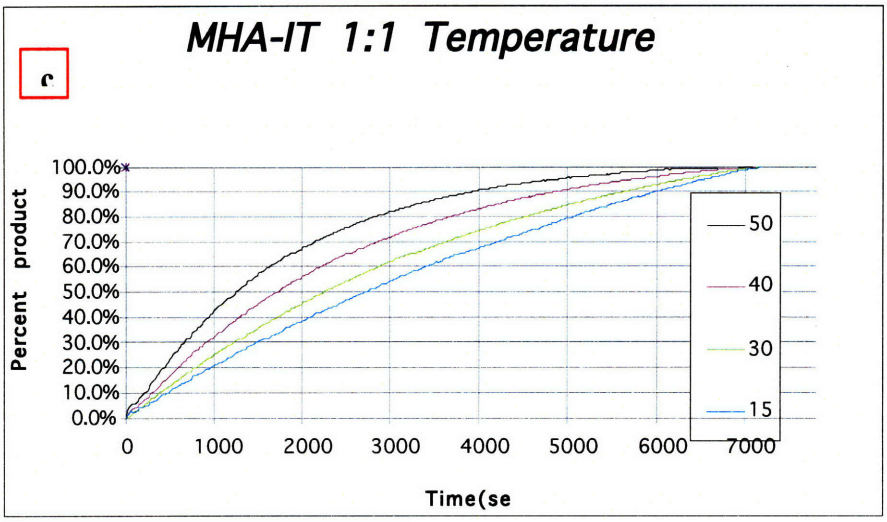

Figure 7: Percent product (normalized) vs. time for a. MHA: IT 1:2 b. MHA: IT 2:1 c. MHA: IT 1:1.

All three plots in Figure 7 demonstrate a quicker increase of percent product formed, and therefore a faster reaction rate, with increased temperature.

By running the temperature trials first with MHA: IT 1:2, it was found that the temperature range yielding usable data for this catalytic reaction was approximately from 15C to 50C. The high temperature curves, each displaying more than one peak, did not result as expected, and because these runs had very little usable data to fit, they were not included on the same plot as the curves. The temperature runs outside of this range are not included in Figure 7 but are presented in Figure 8 below.

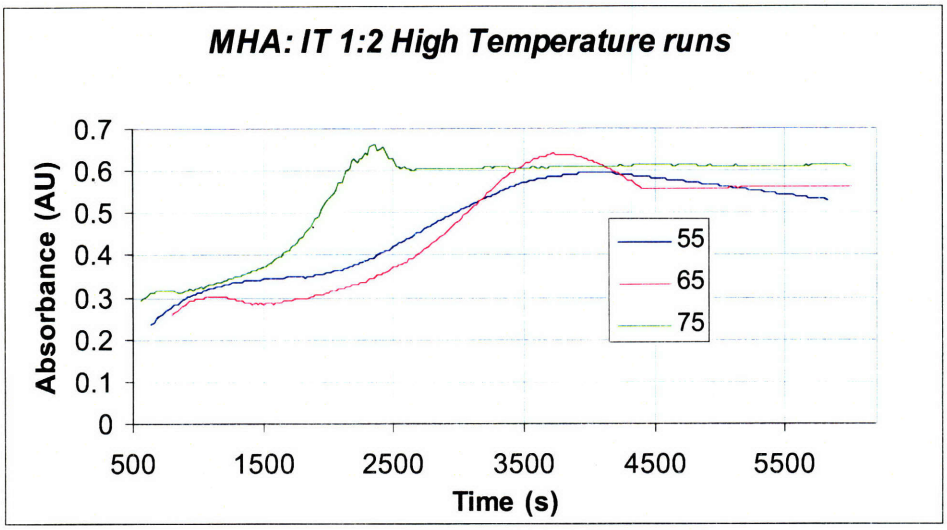

Figure 8: Catalytic runs for MHA: IT 1:2 at temperatures outside of usable temperature range.

As seen for the 55C, 65C, and 75C temperature runs with MHA: IT 1:2, there seems to be another peak forming as well as an inflection in the curve rather than the normal expected convex curve and consequential leveling out found in the other temperature trials. (Because of these results, the same successful temperature of 15C to 50C was used for the catalytic trials with MHA: IT 2:1 and 1:1.) In order to investigate this phenomenon, two 75C trials were run again, one without the DNPA and one without the catalyst. By running these two trials, it was possible to see the individual effect of each component with the buffer at 75C during the run on the UV-VIS spectrometer. These additional 75C trials are provided in Figure 9.

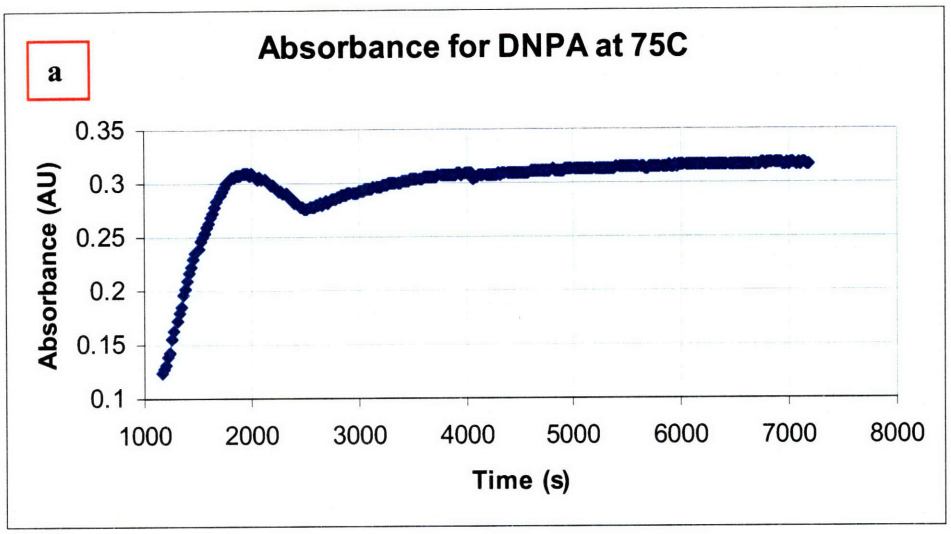

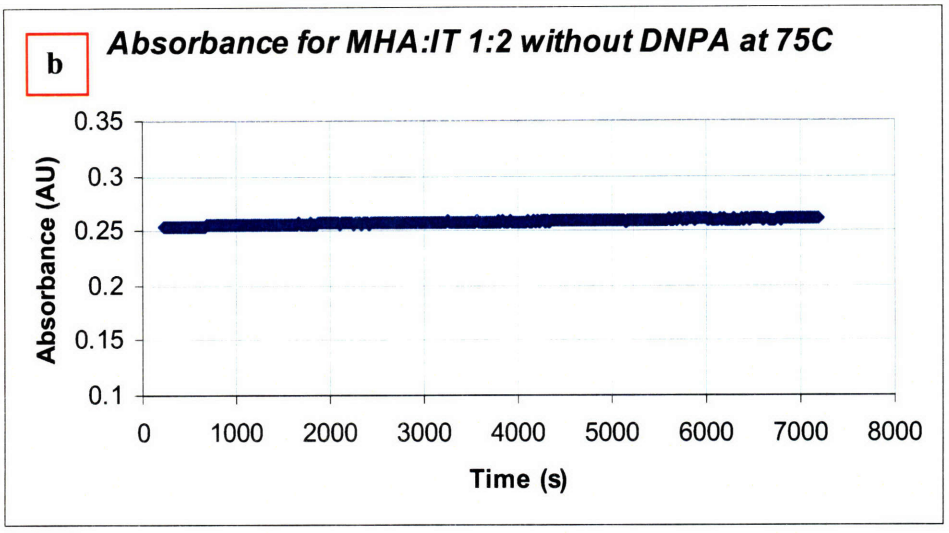

Figure 9: MHA: IT 1:2 at 75C a. without catalyst and b. without DNPA

From the two 75C runs shown in Figure 9, it is clear that the strange results obtained at these higher temperatures are due to some activity with the DNPA and not the catalyst, since the run without the DNPA is flat and shows no activity.

The time constant t values obtained from the fitting of the temperature trial curves in Figure 7 as well as the corresponding k_{cat} values that were calculated are provided in Table 2 below. All fitted curves had an R^2 value of at least 0.99. In addition, the

calculated extinction coefficient values for the systems of MHA: IT 1:2, 2:1, and 1:1 were 1.37×10^7, 4.26×10^6, and 2.98×10^7 respectively. It is important to note that a second order equation was used to fit the 1:2 series whereas a first order equation was used to fit the 2:1 and 1:1 series.

	MHA: IT 1:2		MHA: IT 2:1		MHA: IT 1:1	
Temp(C)	**t(s)**	**k_{cat}(1/Ms)**	**t(s)**	**k_{cat}(1/Ms)**	**t(s)**	**k_{cat}(1/Ms)**
15	609.5	95.67	2011.30	21.51	7200	883.43
25	498.9	115.87	1441.23	30.33	--	--
30	352.95	112.10	1197.70	36.13	4252.9	1419.43
35	506.04	123.74	--	--	--	--
40	240,2	151.51	867.43	51.58	2681.2	2370.65
45	406.39	154.11	--	--	--	--
50	203.0	195.13	791.36	56.04	1832.53	2767.88
60	--	--	554.66	77.42	--	--
70	--	--	466.57	94.42	--	--
80	--	--	353.01	126.28	--	--

Table 2: Kinetic parameters obtained for MHA: IT 1:2, 2:1, and 1:1

In order to fit these curves effectively, some portions of data were removed to obtain a better curve. These data include the lead-in points up to the jumping point when the DNPA is added to the system as well as some other minor blips in the curves. The exact times for where the data was spliced out for each curve are summarized in table format in the appendix. These k-values further support the trend that was evident in Figure 7: an increase in rate constant occurs with an increase in temperature. Figure 10 presents the

Arrhenius plots created from the k_{cat} and temperature data sets obtained from the catalysis temperature trials run with the 1:2, 2:1, and 1:1 nanoparticle syntheses.

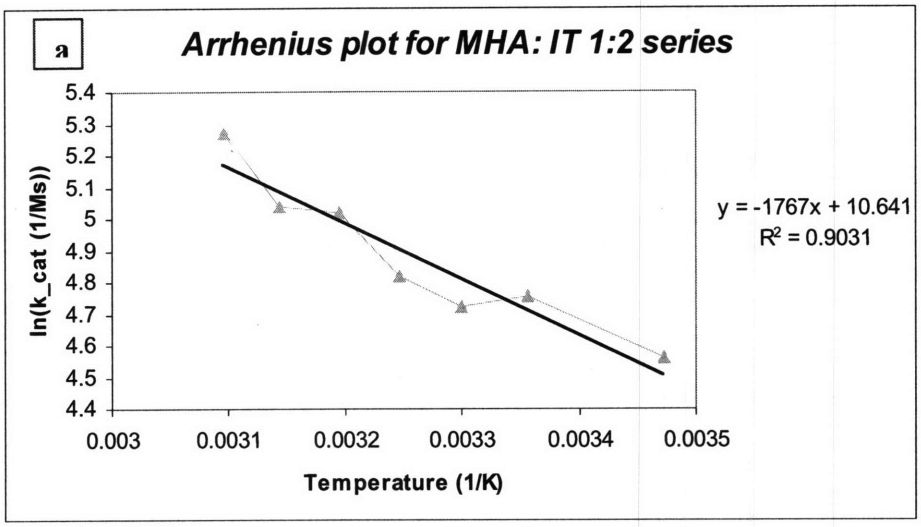

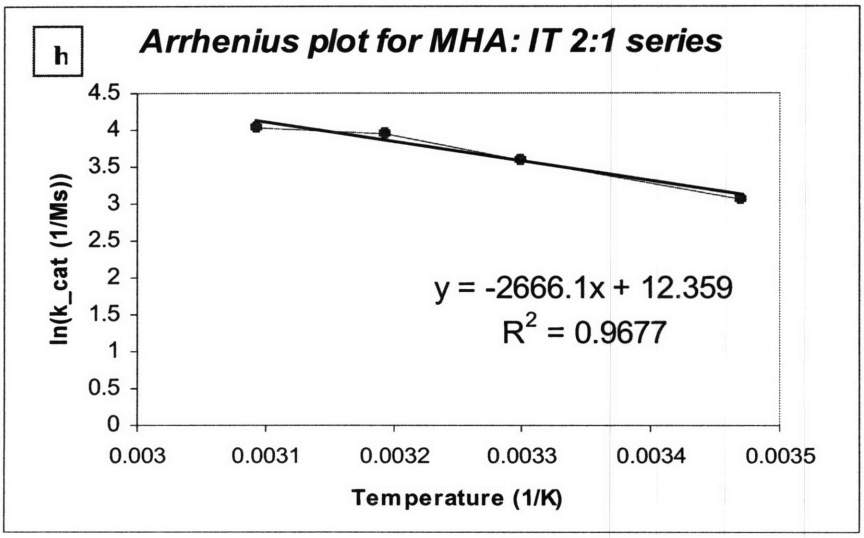

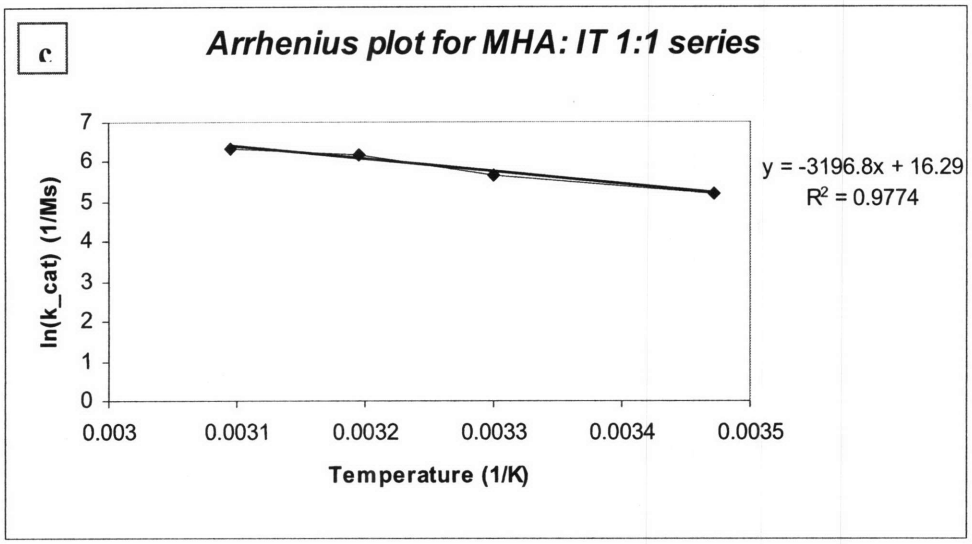

Figure 10: Arrhenius plots of catalysis reaction with a. MHA: IT 1:2 b. MHA: IT 2:1 c. MHA: IT 1:1.

Trend lines, along with their equation and R^2 values, are included in the Arrhenius plots. The R^2 values are no lower than 0.90 which demonstrates that the data is fairly linear. The activation energy for the MHA: IT catalysis reactions for 1:2, 2:1, and 1:1 are shown in Table 3 below.

.

MHA: IT	Ea (kJ/mol)
1:2	14.70
1:1	26.52
2:1	22.17

Table 3: Activation energy values for MHA: IT 1:1, 1:2, and 2:1

6. Discussion

The control run of 1-butylimidazole in H_2O (Fig. 5) successfully reproduced Scrimin, *et al.*'s curve presented in Figure 3. This reproduced curve provides reassurance that the catalytic hydrolysis reaction takes place.

The kinetic curve obtained for the1-butylimidazole control run successfully reproduced Scrimin's control curve shown in Figure 3. The catalytic runs performed at a range of pHs prove to be inconsequential since the overall curve did not behave similarly to that of Scrimin's top curve in Figure 3. This contrasting result, therefore, points out that the variation of pH does not influence the rate of reaction in a uniform way.

The plot of catalytic reactions tested over a range of pHs (Fig. 6) shows no specific pH range at which there occurs a distinct peak in rate constant value. Because these trials with the bi-ligand nanoparticles did not display the peak in k values that was found for the Scrimin catalytic system, it was decided that looking into the relationship between the catalytic performance and the pH of the system did not display a conclusive trend for pH and the most favorable value for the better k values.

The kinetic curves and corresponding k values obtained for MHA: IT 1:2, 2:1, and 1:1 over a range of temperatures (Fig. 7) demonstrate the expected direct relationship between reaction rate and temperature. An increase in the rate constant can be seen when the catalytic reaction is run at a higher temperature. As mentioned in the results section, the catalyst runs performed for MHA: IT 1:2 above 50C displayed unexpected curves with a seemingly secondary reaction occurring (the second peak) and the runs below 15C did not return curves large enough to analyze. Therefore, the suitable temperature range

to perform this catalytic reaction with these nanoparticles was initially concluded to be approximately 15C to 50C. It is clear from the trials shown in Figure 9 that the unexpected shape of the curves for 55C, 65C, and 75C is a result of some activity with the DNPA and not something occurring with the catalyst because of the strange curve obtained when running just the buffer solution with DNPA.

In addition to the secondary curve present in the higher temperature runs, all of the MHA: IT 1:2 curves straighten out at the end but rise in an almost perfectly linear manner instead of leveling off to a completely flat and approximately horizontal line as should be expected at the end of the catalytic reaction. Because kinetic curves obtained of past runs on alternative UV-VIS spectrometer machines displayed curves that flattened out to a horizontal line without a drift, it was initially assumed that this drift was caused by the particular machine being used. However, upon further thought, it was hypothesized that these curves with a drift for the 1:2 series might be due to diffusion of the DNPA added to the catalyst solution in the cuvette. After completing one of the 1:2 runs, the solution in the cuvette did not look uniform, hinting to the possibility that the DNPA was not mixed thoroughly into the catalyst solution when added during the catalyst run. Therefore, the resulting wave in some of the curves could be a diffusion wave of highly concentrated DNPA flowing into the beam path and swamping the signal. This theory makes sense with the obtained data – the wave phenomenon seems to have a larger effect and appear more prominently at higher temperatures. This fact correlates with the property of diffusion occurring faster at higher temperatures. (Perhaps a wave in the curves at lower temperatures was not seen because the run was not left on long enough to monitor the slower diffusion of the DNPA.) The 2:1 and 1:1 series were

conducted under a procedure that was updated to thoroughly mix the DNPA into the cuvette solution by turning the cuvette upside down and then right side up several times. The 2:1 and 1:1 catalytic trials produced curves without any drift – thus supporting the current hypothesis that the previous drift experienced was due to insufficient mixing of DNPA into solution. While this diffusion theory calls into question the concentrations calculated for some of the 1:2 catalytic runs, the curves still demonstrate the trend of an increased k rate with an increase in temperature.

The kinetic curves obtained for the 2:1 series are as expected. While the kinetic curves for the 1:1 series demonstrates the expected trend, the shape of the curves do not resemble exactly the same form as the other two series. Instead of a more upside down L-shaped curve with a quick rise and leveling off, the 1:1 curves have a more C-shaped curve with a more gradual rise and eventual flattening.

As mentioned in the results, the equation used to fit the kinetic curves for MHA: IT 1:2 was of second order rate form and the fitting therefore returned two time constants, t_1 and t_2. By reviewing both time constant values for the 1:2 nanoparticle runs, it is evident that the t_2 values are on the expected order of magnitude and they decrease with increase in temperature, as was expected. In contrast, the t_1 values are several orders of magnitude larger than their corresponding t_2 values and they all increase with an increase in temperature. Because these t_1 values are extremely large and they also unreasonably increase with an increase in temperature, it is assumed that these values are not real and the t_2 values are valid values. The better fitting results when using the second order equation could be due to the drift that is evident in most of the kinetic curves produced for the 1:2 series. Especially since it was possible to use a first order equation to fit the

curves that did not experience any drifting (the 2:1 and 1:1 data series), it is clear that the drifting experienced for the 1:2 series affects the fitting of the curves.

The k_{cat} values provided in Table 2 confirm its trend with temperature as well as surface morphology. For a given ligand-ratio system, all the rate values increase with increased temperatures. In addition, the overall rates for the 1:1 system are the fastest, followed by those for the 1:2 and then 2:1. This trend of k_{cat} values among different ligand-ratio systems of MHA: IT agree with the initial trend found for these systems at 25C (Fig. 4).

The activation energy values provided in Table 3 were not all as expected – the Ea value for 1:2 relative to 2:1 was as predicted, but the Ea value for 1:1 was not anticipated. The Ea value obtained for the 2:1 series at 22.17 kJ/mol was larger than the Ea value for 1:2 at 14.7 kJ/mol. Surprisingly, the Ea value for the 1:1 series was found to be the largest of the three at a value of 26.52 kJ/mol. This Ea trend obtained for varying ligand composition correlates with the catalytic rate constants for the 2:1 and 1:2 MHA: IT systems presented in Figure 4; however, it does not match up with the catalytic rate constant obtained for 1:1 MHA: IT. Because the 1:1 system demonstrated the highest catalytic rate constant, it was expected to result in the smallest activation energy value, not the largest value. The fact that the 2:1 series possessed a larger activation energy value than the 1:2 series makes sense with the point that the 2:1 series also has been found to have a slower catalytic rate than that of the 1:2 series. Moreover, the 1:1 series aside, a ligand ratio system with a faster catalytic rate constant was demonstrated to have a smaller activation energy value. This trend between the 2:1 and 1:2 series makes sense because a reaction will be able to go to completion faster if the activation energy is lower

and therefore easier to overcome. However, the very large Ea value for the 1:1 series seems counterintuitive. The Ea result obtained for the 1:1 series seems to be inaccurate because the k_{cat} values are very large and also off by an order of magnitude compared with previously measured values for k_{cat} of the 1:1 MHA: IT system at 25C. This fact suggests the need to reproduce the 1:1 MHA: IT series and see if the results are different and more similar to what was originally expected. The previous k_{cat} data for the 1:1 MHA: IT series at 25C was obtained using a different catalyst concentration than what was used for this project – perhaps these suspicious data is a result of using a different catalyst concentration. However, in the case that the data obtained for the 1:1 series is not due to some error, then there are many interesting findings to be noted about this catalyst system. Assuming the results are accurate for the 1:1 series, the $t_{attempt}$ values are very high (the time is very short), and the very high catalytic rate constants are very favorable in terms of kinetics, but these 1:1 nanoparticles are unfavorable in terms of energetics. This trend is very strange and unprecedented for a catalyst but, if accurate, could lead to some very interesting consequences and applications.

Overall, it is important to note a few assumptions made for this project: the bi-ligand nanoparticles in all three systems explored are rippled, and the ratio of ligands added to the nanoparticle synthesis is the same as what is actually on the nanoparticles. It is also important to consider that the kinetic rates obtained could be slightly inaccurate because of an error in concentration value that was calculated, possible hydrolysis of the stock DNPA that was used, as well as incomplete mixing of the solution used during catalytic testing.

7. Conclusion and Future Work

The effect of temperature on the catalytic reaction of MHA: IT with DNPA was successfully demonstrated. As expected, the direct relationship between reaction rate and temperature was found. For all three ligand ratio systems tested, it was demonstrated that the catalytic rate constant increased with an increase in temperature. It was also found that by improving the procedural methods of mixing the DNPA into the catalytic solution during UV-VIS monitoring, more accurate curves were obtained with no drift or wave phenomenon. The activation energy values were found for the three ligand-ratio systems and the values for the 2:1 and 1:1 series were found to correspond to the catalytic rate constant trend previously obtained at 25C -- the activation energy value was lower for the 1:2 series, the system that displayed higher catalytic reaction rates. In contrast, the activation energy value for the 1:1 series was found to be the largest out of the three systems tested and it did not correspond with the catalytic rate constant versus composition trend. This project showcases the preliminary testing of this MHA: IT system with varying temperature. Therefore, while the 1:1 data is most likely attributed to some error source, it seems that most of the kinks of the experimental procedure are solved and future reproduction of these data series are likely to be highly more accurate.

While the reason behind the particular trend of faster reaction rates and corresponding activation energy values for specific ratios of surface ligands (for the 2:1 and 1:1 systems) as well as the overall higher reaction rates for the MHA: IT system compared to other ones is not yet understood, there is a possible hypothesis. The MHA: IT surface composition gives a more structured surface to the gold nanoparticles which

might be more conducive to catalysis. It makes sense that the 1:1 system gives the fastest kinetic results because it is the most ordered and structured one. It has the smallest as well as highest number of domains compared to the 1:2 and 2:1 systems which are less structured. It is possible that the MHA: IT system performs better overall compared to other bi-ligand systems because the catalyst sited on the surface along with the longer MHA ligands creates a tight pocket that restricts the allowable conformations and allows for better, more specific catalysis.

While several informative trends were found as a result of this project, there are many future considerations that can be taken in order to strengthen and further investigate these findings. Because of the diffusion and curve drift concern with the 1:2 ligand-ratio series, it would be useful to reproduce the results with the updated procedure of thorough mixing of DNPA as well as to set up these runs at an increased number of temperatures. This step would lead to more accurate results for kinetic rate and activation energy values. Also, in order to understand the Ea result for 1:1 more fully, the catalytic runs should be repeated using the same catalyst concentration as previous runs in order to equilibrate across systems and reduce any areas of difference, and therefore possible errors, between runs. It would also be interesting to compare other kinetic parameters, such as the jump frequency, as well as to obtain Ea values for other rippled nanoparticle systems and explore the resulting trend of Ea values with ligand ratios.

In order to further ensure more accurate data, it might prove useful to set up a blank run of only the buffer with water in order to measure the k rate due to water interaction; this value could then be subtracted from the observed reaction rate in order to get a more accurate rate constant value due solely to the catalyst.

In the future, reproducing these results and obtaining more accurate data as well as data for other systems might lead to a more concrete explanation of why the specific surface morphologies for the MHA: IT system behave more favorably as catalysts than others. These findings could lead to a better understanding of how to optimize the rippled nanoparticle system as a catalyst, determine what specific surface morphology helps to create the most efficient catalyst, and learn how these rippled nanoparticles may be used to model and more fully understand the behavior of enzymes.

8. Appendices

8.1 Chemical drawings of the pertinent ligands

2,4-dinitrophenyl acetate (DNPA)

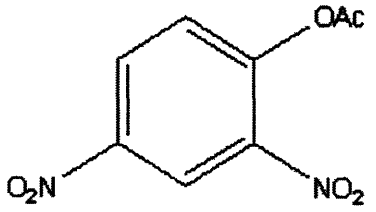

16-mercapto-hexadecanoic acid (MHA)

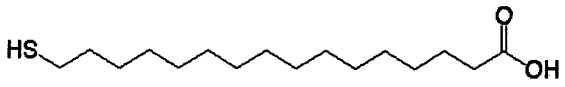

1-octanethiol (OT)

8.2 Table of chemical manufacturers

Chemical	Manufacturer
HEPES buffer	Sigma Aldrich
MES buffer solution	Biochemika

8.3 Table of kinetic curve data used for fitting 1:2 series

Temperature	Data range used
15	741.9-7181.8
25	92-7171.2
30	481.9-7181.8
35	722-7181.8
40	662-2461.9
45	661.9-5441.8
50	841.9-2501.9

References

1. Jackson, A.M.; Myerson, J.W.; Stellacci, F. *Spontaneous assembly of sub-nanometre ordered domains in the ligand shell of monolayer protected nanoparticles*. Nat. Mat. 2004, 3, 330-336.

2. Copeland, Robert A. *Enzymes: A Practical Introduction to Structure, Mechanism, and Data Analysis*. Wiley-VCH, Inc. 2000.

3. Engel, T. and Reid, P. *Physical Chemistry*. Pearson Education Inc. 2006.

4. Pasquato, L.; Rancan, F.; Scrimin, P.; Mancin, F.; Frigeri, C. *Chem. Commun.* 2000, 2253-2254.

5. Courtesy of original research by Benjamin Wuensch, Department of Materials Science and Engineering, Building 13 4th Floor 77 Massachusetts Avenue, Cambridge, MA 02139.

6. Courtesy of original research by Jeffrey Kuna, Department of Materials Science and Engineering, Building 13 4th Floor, 77 Massachusetts Avenue, Cambridge, MA 02139

7. Bugg, T.D.H. *Introduction to Enzyme and Coenzyme Chemistry*. Blackwell Publishing. 2004.